JOURNAL OF GEOPHYSICAL RESEARCH, VOL. 100, NO. B3, PAGES 3929–3941, MARCH 10, 1995

Measurement and interpretation of tidal tilts in a small array

M. L. Kohl[1] and J. Levine[2]

Joint Institute for Laboratory Astrophysics, University of Colorado, Boulder

Abstract. Strain-induced tilts caused by variations in material properties can produce large perturbations in the tilt field near a material discontinuity. This is evidenced in data from a closely spaced array of borehole tiltmeters that has been operating at Piñon Flat Geophysical Observatory in southern California since 1987. The array is composed of three borehole tiltmeters located at depths of 24, 36, and 120 m. The tiltmeters have a sensitivity of a few nanoradians. Tidal measurements show differences between the boreholes of up to 50%. The largest percent difference occurs in the semidiurnal band where the tilt field measured in the 36-m borehole differs by ~10 nrad at the M_2 frequency. This difference has been modeled as a strain-induced tilt caused by the weathering layer.

Introduction

Measurements of the deformation of the Earth are generally complex functions of the direct response of the Earth to the deforming forces combined with instrument response, surface loading, and local crustal structure. Because the driving forces and frequencies of tides are well known globally, solid Earth tidal measurements can be used to investigate the effects of instrument response, surface loading, and local crustal structure. Proper interpretation of measured deformations requires that each of these effects are understood.

The instrument response includes not only the mechanical and electrical characteristics of the instrument but also the coupling mechanism between the instrument and the Earth. Many early tilt and strain measurements were made inside mines or tunnels and significant discrepancies between nearby instruments were observed at tidal frequencies. The source of these discrepancies has largely been attributed to how the instrument was coupled to the Earth. *King and Bilham* [1973] and *Harrison* [1976] showed that local strain-induced tilts arise from the presence of a cavity (or other local heterogeneities), and care must be taken to locate a tidal instrument to reduce this effect as much as possible.

Surface load deformations also contribute to tidal measurements. The tidal response of the oceans and atmosphere combines with the direct response of the Earth and varies with location. In addition, the instruments respond to surface deformations associated with near surface weathering and thermo-elastic effects [*Wood and King,* 1977, *Wyatt et al.,* 1988].

Local crustal structure can also influence tidal measurements. *Beaumont and Berger* [1974] predicted that dilatancy before an Earthquake will cause spatial and temporal changes in the response of the Earth at tidal frequencies. They also showed that the amplitude and phase of the Earth tides near the boundary of two elastic regions would vary with position. Arrays of instruments could be used to map lateral variations in the local structure, particularly when the loading is equivalent for all the instruments in the array [*Beaumont,* 1978, *Meertens et al.,* 1989, *Peters and Beaumont,* 1987].

This paper reports on results from a closely spaced array of borehole tiltmeters at Piñon Flat Geophysical Observatory in southern California. The array initially was composed of two boreholes; BOA 24 m deep (above the water level), and BOB 35 m deep (below the water level). The first installations of these two boreholes showed large discrepancies in the tidal signal. BOC was then drilled to 120 m depth, far below the water level and in more homogeneous material. There were three installations of BOA and BOB and two installations of BOC. The results are summarized in Tables 2 and 3. Modeling of the local crustal inhomogeneities led to modifications of the tiltmeter capsule. The modified capsules were installed in BOA and BOB (installations 4 and 5) and data from this experiment are summarized in Tables 6 and 7. Piñon Flat Geophysical Observatory (see Figure 1) was chosen as an ideal test facility for the array since many geophysical instruments are located there.

Instrumentation

A detailed description of the borehole tiltmeter is given by *Kohl and Levine* [1993]. The tiltmeter con-

[1]Now at Timing Solutions Corporation, Boulder, Colorado.

[2]Also at Time and Frequency Division, National Institute of Standards and Technology, Boulder, Colorado.

Paper number 94JB02773.
0148-0227/95/94JB-02773$05.00

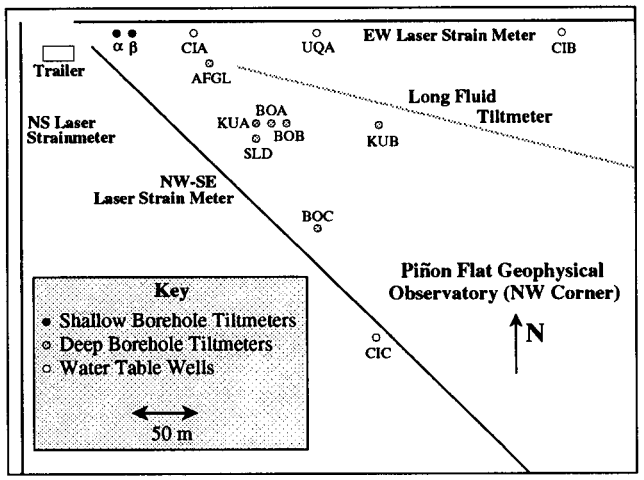

Figure 1. Schematic drawing of Piñon Flat Observatory near the deep borehole tiltmeter array. Individual instruments are discussed in the text.

tains a pair of orthogonal horizontal pendula that are mounted in a sealed sensor package with a leveling range of ±5°. The sensor is clamped to the inside of a watertight capsule that is lowered into the borehole. The displacement of each pendulum is determined using a capacitive transducer which produces a dc voltage tilt signal. The tilt signals are sent through a low-pass filter with about a 100-s time constant to average out microseismic background noise. The filtered signals are recorded every 6 minutes on a data logger at the site. Aliasing is not a problem because there is very little energy at periods shorter than the Nyquist 720 s. The digitized data are retrieved each morning by an automatic dialing program [*Levine*, 1983]. The overall sensitivity of each pendulum is set to be about 2V/μrad. Successive calibrations agree at the 1% level even when spaced several years apart [*Levine et al.*, 1989]. For the nominal sensitivity of 2V/μrad, the least count of the digitizer is about 2.4 nrad.

Figure 2 shows a schematic drawing of the borehole. A conical joint connects the 10-cm-diameter instrument compartment with 15-cm-diameter casing pipe. The casing pipe is cemented along its entire length to the surrounding material.

All versions of the tiltmeter capsule were made from 2-m-long stainless steel pipe sections, and the baseline length of the measurement is therefore 2 m. Figure 2 shows the original capsule located in the borehole. This design was chosen to eliminate all cavity effects from measuring in a borehole [*Harrison*, 1976]. The other versions are modifications of this design and will be described later.

The capsule is lowered into the borehole by a steel cable connected to the lid. The orientation of the capsule at the bottom of the borehole is determined differently depending on the depth of the borehole. A series of light-weight aluminum rods is used to translate the orientation of the capsule to the surface for relatively shallow boreholes ($\leq$ 36 m). The azimuth of the sensors is then determined using a compass. This method generally determines the orientation within ±5°. For deeper holes, the lid of the capsule was modified to include an extension with a muleshoe. As the capsule is lowered, the muleshoe reaches a key welded to the inside of the casing. The orientation of the key is determined by attaching a gyroscope to the muleshoe. Once the azimuth of the key is known in a borehole, the azimuth of subsequent installations can be determined knowing the orientation of the sensor with respect to the muleshoe. The azimuth uncertainty using this method was 2°.

Site

Piñon Flat Geophysical Observatory is located in the Santa Rosa Mountains of southern California approximately 100 km from the Pacific Ocean and 250 km from the Gulf of California at 33.64°N and 116.46°W [*Wyatt*, 1982]. It is about 12 km northeast of the San Jacinto fault system and 25 km southwest of the San Andreas fault zone on a block which is generally devoid of microseismicity [*Fletcher et al.*, 1990]. The observatory is located on a southerly facing flank of Asbestos Mountain with Deep Canyon to the east of the observatory, Santa Rosa Mountain to the south, and Palm Canyon to the west. The site is inclined about 2.5° to the southwest at an altitude of ≈1274 m.

The flat is roughly 12 km^2 and is situated on granitic material. The upper 0.3 m is a layer of sand which covers crystalline rock composed of granodiorite. The rock is rich in biotite which results in rapid weathering when the rock is exposed to moisture [*Wyatt*, 1982]. This produces a weathered layer of decomposed granite.

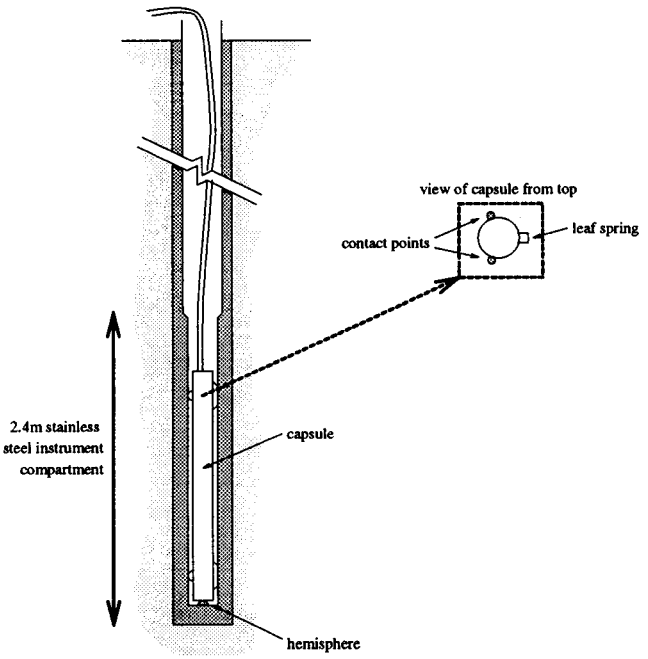

Figure 2. Schematic drawing of the borehole with the original capsule installed. The capsule rests on a hemisphere at the bottom of the borehole. A flat spring at the top and bottom of the capsule presses the contact points against the sides of the borehole.

Stierman and Healy [1984] studied the weathering layer at a site similar to Piñon Flat. They noted that the change from weakened to competent rock could be quite abrupt, occurring in the region above the water table.

It is not unusual to find large discrepancies in the water depth over short baselengths at Piñon because of the fractured granite. There are four wells drilled at Piñon for monitoring the water level (labeled CIA, CIB, CIC, and UQA in Figure 1). The mean altitude of the water depth varies by 14 m between the wells. CIA was logged during drilling in 1981 and water was reached at 36 m depth [*Evans and Wyatt,* 1984].

Wyatt [1989] conducted an extensive survey of data collected at Piñon Flat to determine the material properties and structure at the site. By using the results of rainfall loading, atmospheric loading, tidal data, and seismic profiling, he determined that Young's modulus and Poisson's ratio jump in value between 15 and 35 m depth.

The Joint Institute for Laboratory Astrophysics deep borehole array is composed of the three boreholes labeled BOA, BOB, and BOC. BOA and BOB were drilled in 1986 and BOC was drilled in 1988. The depth of the boreholes varies; BOA is nominally 24 m deep, BOB is 35 m deep, and BOC is 120 m deep. The water level is believed to be below BOA and above BOB, but no record of the water level was kept when the boreholes were drilled. The two shallow holes are located about 15 m apart along an E-W direction. BOC is located about 20 m to the east and 90 m to the south of BOB. The locations were chosen to augment an existing array of other borehole tiltmeters at the site.

Data and results from several of the other instruments shown in Figure 1 have been used in the interpretation of the tilt data from our deep borehole array. In particular, temperature and barometric pressure recorded every 5 min at the trailer were compared with the tilt data to determine if they were affecting the tilt measurements. Water level fluctuations measured in the wells labeled UQA, CIA, CIB, and CIC were also used. The strain field measured at the site by the laser strain meters [*Agnew,* 1979] (Table 1) was used as the local strain field.

Tidal Data

Data have been collected since early 1987 from the two shallowest holes, BOA and BOB. BOC had a tiltmeter installed in 1989. Figure 3 shows a typical time series from BOA during 1991. The sensor had a drift rate of about 1 μrad/yr, which was an average rate at

Table 1. O_1 and M_2 Strain Tides Measured at Piñon Flat With the Laser Strain Meters

Azimuth, deg	O_1 Amplitude, nε	O_1 Phase, deg	M_2 Amplitude, nε	M_2 Phase, deg
0	3.58	-8.6	12.21	0.8
90	5.08	8.9	5.37	-20.2
135	4.71	11.4	12.63	-0.1

From Agnew [1979].

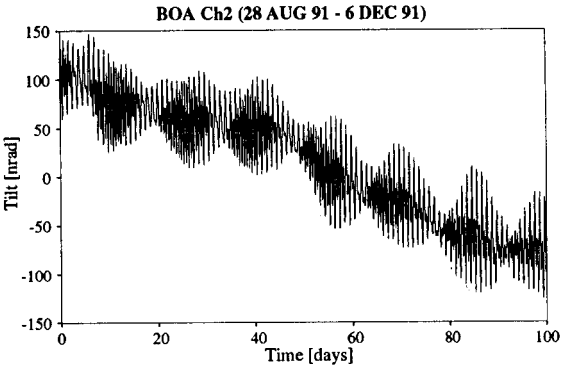

Figure 3. Typical time series from 24-m borehole. The drift of the instrument has not been removed.

Piñon. The power spectral density of the data during this interval is shown in Figure 4. Both the raw data and the residuals (drift and tides removed) are shown. The amplitudes and phases of the tidal components were determined using the tables of *Cartwright and Taylor* [1971] with the corrections of *Cartwright and Edden* [1973]. Sixteen groups of all terms that exceed 0.1% of the tidal potential were fit to the time series after the drift was removed. Each group consisted of those frequencies within 1 cycle/month of each other. Table 2 shows the M_2 tides for the initial installations of each of the holes. Table 3 shows the O_1 tides for the same installations. The results are not sensitive to the length of the time series. All of the data in these tables was obtained using the original capsule design. The data interval (column 2) indicates the first and last day of data used to obtain the tidal parameters and typically contains brief periods where no data were available. The numbers in parentheses are the uncertainties in the fit of the data, which do not include the calibration uncertainties listed separately. The phases are determined with respect to the phase of the tidal potential, where a negative phase implies a phase lead.

The tidal ellipse for a particular tidal frequency is the graphical presentation of the tidal amplitudes and phases at that frequency. It is essentially a phasor diagram where the amplitude and phase along a particular azimuth is plotted as the endpoint of a vector. The length of the vector corresponds to the amplitude of the tide along that azimuth and the angle from the real

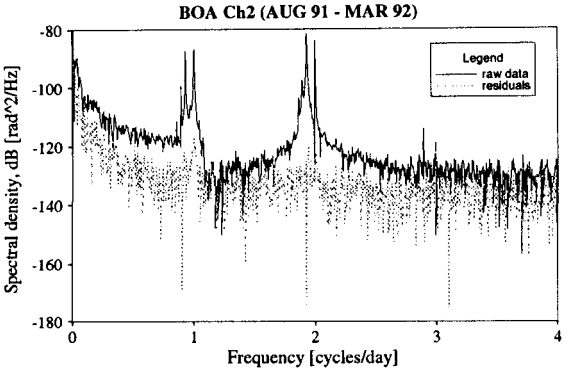

Figure 4. Power spectral density of data from the 24-m borehole. The raw data include the drift of the instrument.

Table 2. M_2 Data

Installation	Data Interval, yr:day	Pendulum 1 Azimuth, deg	Pendulum 1 Amplitude, nrad	Pendulum 1 Phase, deg	Pendulum 2 Azimuth, deg	Pendulum 2 Amplitude, nrad	Pendulum 2 Phase, deg	Uncertainty, % Ch1	Uncertainty, % Ch2
				BOA					
1	87:021—87:250	328	25.33 (0.11)	108.8 (6.0)	58	7.08 (0.25)	-138.0 (4.7)	—	—
2	88:202—91:213	97	18.19 (0.23)	-83.3 (0.6)	7	18.72 (0.34)	124.0 (0.6)	3.5	2.5
3	91:215—92:067	49	6.47 (0.15)	-175.7 (1.3)	319	24.79 (0.37)	107.4 (0.9)	3.5	2.5
				BOB					
1	87:001—87:217	353	20.34 (0.18)	98.5 (1.5)	263	13.32 (0.25)	70.1 (1.1)	—	—
2	89:114—91:213	87	15.94 (0.64)	-110.0 (1.8)	357	20.05 (0.47)	98.6 (2.4)	1	1
3	91:215—92:067	296	22.90 (0.62)	86.3 (1.6)	206	10.39 (0.22)	-66.9 (1.2)	1	1
				BOC					
1	89:344—90:205	35	11.18 (0.76)	151.8 (3.9)	125	22.81 (0.83)	-75.3 (2.1)	1	1
2	90:251—90:279	35	12.66 (0.42)	153.9 (1.9)	125	23.51 (0.35)	-77.1 (0.9)	1	1
				*Theoretical tide**					
		0	27.38	129.3	90	19.67	-100.1		

Values shown in parentheses are the uncertainties in the fit of the data. Uncertainties in the calibration of the first installation were assumed to be 3.5% (worst case) when needed.

* Including topography [*Kohl*, 1993]

axis corresponds to the phase of the tide measured with respect to the phase of the local potential. Hence the real part refers to the tilt signal that is in phase with the tidal potential. The amplitude and phase of the tilt along an arbitrary azimuth can be determined in terms of the amplitudes and phases of the tilt along any two orthogonal axes [*Levine et al.*, 1989]. Let A_1 and ϕ_1 be the amplitude and phase of the tilt along azimuth α, and A_2 and ϕ_2 be the amplitude and phase along azimuth $\alpha + 90$. Then the amplitude and phase of the tilt along β is

$$A_\beta^2 = A_1^2 \cos^2(\beta - \alpha) + A_2^2 \sin^2(\beta - \alpha) + 2A_1 A_2 \cos(\phi_2 - \phi_1) \cos(\beta - \alpha) \sin(\beta - \alpha) \quad (1)$$

$$\phi_\beta = \tan^{-1}\left(\frac{A_1 \sin\phi_1 \cos(\beta - \alpha) + A_2 \sin\phi_2 \sin(\beta - \alpha)}{A_1 \cos\phi_1 \cos(\beta - \alpha) + A_2 \cos\phi_2 \sin(\beta - \alpha)}\right) \quad (2)$$

Using the tidal amplitudes and phases along two orthogonal azimuths, the amplitudes and phases along every other azimuth can be calculated and plotted producing the tidal ellipse.

Table 3. O_1 Data

Installation	Data Interval, yr:day	Pendulum 1 Azimuth, deg	Pendulum 1 Amplitude, nrad	Pendulum 1 Phase, deg	Pendulum 2 Azimuth, deg	Pendulum 2 Amplitude, nrad	Pendulum 2 Phase, deg	Uncertainty, % Ch1	Uncertainty, % Ch2
				BOA					
1	87:021—87:250	328	5.91 (0.06)	56.4 (4.2)	58	26.22 (0.07)	-80.0 (2.3)	—	—
2	88:202—91:213	97	22.40 (0.41)	-87.3 (1.1)	7	12.11 (0.60)	-70.4 (1.4)	3.5	2.5
3	91:215—92:067	49	24.32 (0.20)	-81.0 (0.5)	319	10.03 (0.25)	80.4 (1.4)	3.5	2.5
				BOB					
1	87:001—87:217	353	8.49 (0.15)	-41.6 (1.8)	263	25.65 (0.27)	91.7 (0.5)	—	—
2	89:114—91:213	87	28.01 (0.17)	-91.1 (1.4)	357	9.00 (0.24)	-50.3 (2.0)	1	1
3	91:215—92:067	296	19.76 (0.43)	81.3 (1.3)	206	20.21 (0.45)	107.4 (1.3)	1	1
				BOC					
1	89:344—90:159	35	20.91 (1.18)	-82.2 (3.2)	125	14.72 (1.20)	-93.4 (4.7)	1	1
2	90:250—90:279	35	22.30 (0.74)	-81.1 (1.9)	125	15.40 (0.80)	-96.0 (3.0)	1	1
				*Theoretical tide**					
		0	9.79	-70.6	90	25.00	-91.0		

Values shown in parenthesis are the uncertainties in the fit of the data. Uncertainties in the calibration of the first installation were assumed to be 3.5% (worst case) when needed.

* Including topography [*Kohl*, 1993]

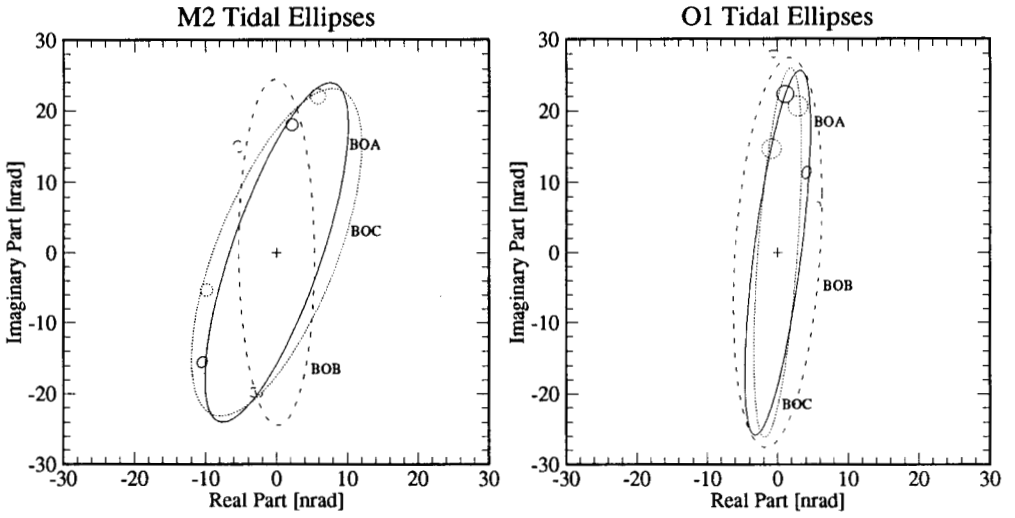

Figure 5. Average tidal ellipses from each of the boreholes using the original capsule design. The small ellipses are the error ellipses for one installation.

The shape of the ellipse is independent of the installation azimuth. The computation of tilt along other azimuths only requires that the two measured azimuths be orthogonal. This implies that it is not even necessary to know the azimuth of the measurement to compare data between instruments at a particular site. The tidal ellipse provides visual comparison of the tilt field, not just a tilt vector.

The tidal data from each borehole have been plotted as tidal ellipses in Figure 5. The ellipses are the average ellipses from the multiple installations of the borehole. The averages were calculated by combining the fits of the different installations weighted by the uncertainties in the measurements. The solid ellipse represents the BOA data, the dashed ellipse represents BOB, and the dotted ellipse is from the BOC borehole. Data from one of the installations for each borehole are shown as error ellipses. It is evident from these plots that the measured tilt field varies significantly between the boreholes. These differences are much larger than expected from measuring at the different depths, or at different locations.

Interpretation

The differences between the measured tilt tides may be caused by several phenomena which can generally

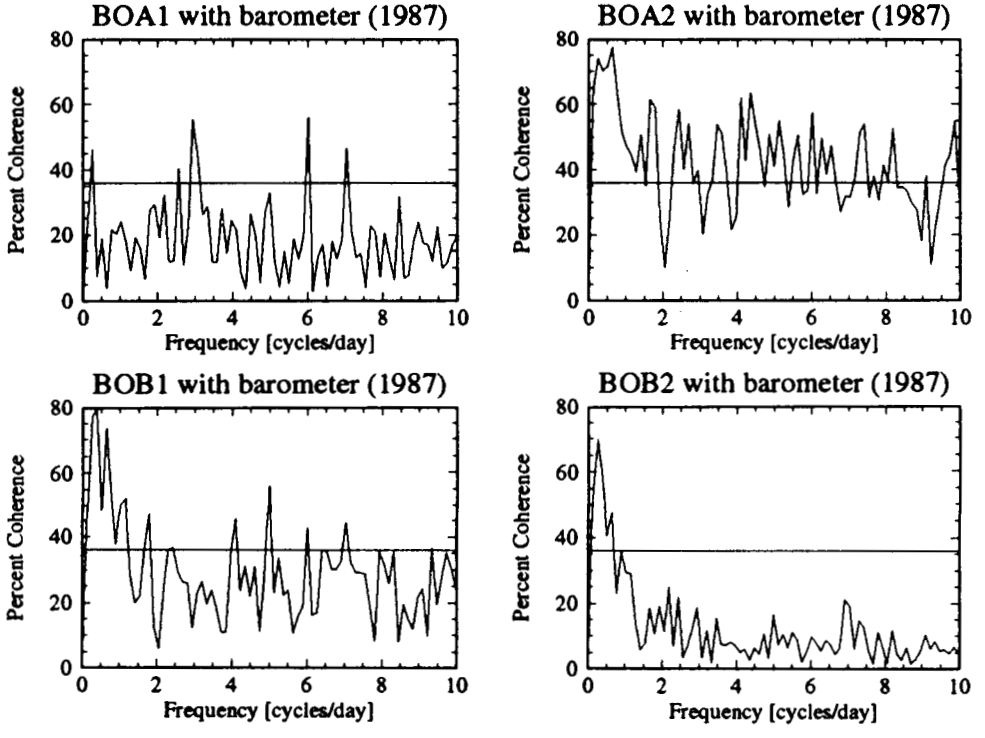

Figure 6. Coherence between tilt and barometric pressure during 1987. The horizontal line indicates the 95% confidence level.

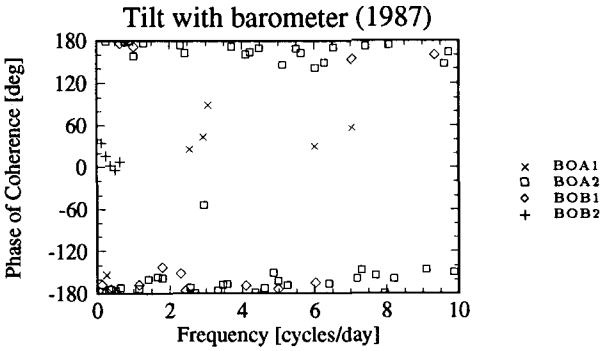

Figure 7. Phase of coherence between tilt and barometric pressure during 1987.

be classified into three categories; environmental, instrumental and material. Environmental effects include the tides induced by environmental variables such as air temperature tides, barometric pressure tides, or tidal fluctuations in the water table level. Instrumental effects arise from the instrument itself; from the way the instrument is mounted to the surrounding material or from the existence of the cavity in which the instrument is placed. Material effects include any perturbations in the tilt field (strain induced tilt tides) caused by local inhomogeneities in the material surrounding the instrument.

Environmental Effects

Continuous records of air temperature, barometric pressure, and water table depths were available between 1987 and 1989. These data were recorded every 300 s.

The coherence and phase spectra between the detided tilt data and the environmental data were calculated using the spectral matrix computed from the Fourier spectra of the two time series. In order to obtain smooth estimates of the spectral matrix elements, the method of segment averaging was used [*Haubrich,* 1965]. Figure 6 shows the coherence amplitude for frequencies less than 10 cycles/day between the barometric pressure and each tilt channel during 1987. (BOA1 indicates BOA channel 1, BOA2 is BOA channel 2, etc.) The horizontal line in the plots indicates the 95% confidence level for coherency. These plots indicate that most of the coherence occurs at low frequencies, less than 1 cycle/day. Figure 7 is the corresponding phase spectrum where the phase of the coherence was plotted for all frequencies when the coherence exceeded the 95% confidence level. This implies that the cause of the coherence is a scalar field (phase of coherence is independent of azimuth) rather than a vector field coupling which would depend on azimuth. The scale factor that minimized the difference between the tilt residuals and the barometric pressure between about 0.1 cycles/day and 0.4 cycles/day was ~70 Pa/nrad. Assuming that the coefficient is frequency independent through the tidal band, a barometrically induced tidal tilt was calculated from the magnitudes of the barometric tidal components. For the O_1 and M_2 tidal frequencies, the barometrically induced tides are well below detectable levels in our instrument.

Data from each of the four water wells CIA, CIB, CIC, and UQA show no coherence with the BOB data and only a limited amount of coherence with the BOA data, and this was correlated with the inverted barometer effect. The temperature also does not directly affect the tilt signal. This is consistent with a simple model of the half-space temperature attenuation of typical rocks as a function of depth [*Agnew,* 1986]. It also indicates that the tiltmeters are installed at sufficient depths to eliminate thermoelastic tilts caused by coupling between the topography and the thermal boundary layer [*Harrison and Herbst,* 1977].

Instrumental Effects

There are several instrumental effects which have been investigated. The first instrumental effect results from the way the capsule references the sides of the borehole. The original capsule referenced only the side of the casing to eliminate cavity effects [*Harrison,* 1976]. However, it referenced the casing in an asymmetric manner, using two contact points and a flat spring spaced 120° apart. The contact points maintain a fixed distance from the inside of the casing while the spring will expand or contract due to deformations of the casing diameter. This can cause a tilt of a capsule located at the bottom of a borehole [*Kohl and Levine,*1993].

This effect was initially calculated using a radially symmetric strain field applied to a two-dimensional cased borehole [*Kohl,* 1993]. The casing has material properties E_1 and ν_1 with an inner radius of R_1 and an outer radius R_2, and the surrounding medium has ma-

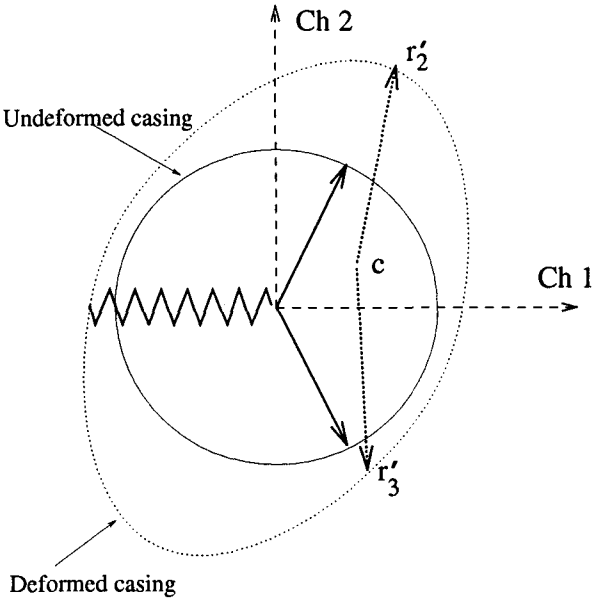

Figure 8. Displacement of the center of the top of the capsule (c) due to the nonuniform deformation of the borehole. The two contact points (r_2, r_3) remain the same distance from the casing walls while the spring expands.

Table 4. Cavity Effect From Asymmetric Spring Effect for All Installations Using the Original Capsule Design

	M_2 x Component		M_2 y Component		O_1 x Component		O_1 y Component	
Installation	nrad	deg	nrad	deg	nrad	deg	nrad	deg
				BOA				
1	0.57	167.0	0.07	21.0	0.39	178.8	0.06	-131.0
2	0.91	177.4	0.22	12.0	0.36	175.7	0.03	76.5
3	1.00	178.1	0.14	-163.5	0.41	-173.8	0.05	44.0
				BOB				
1	0.60	167.4	0.14	-169.7	0.42	-175.7	0.05	-118.3
2	0.98	178.4	0.17	11.0	0.36	177.6	0.04	65.0
3	0.75	174.0	0.25	14.0	0.36	174.2	0.02	-176.2
				BOC				
all	0.91	176.4	0.23	-165.4	0.42	-172.3	0.03	30.8

The x component refers to the effect along the spring azimuth and the y component is the effect orthogonal to the spring azimuth.

terial properties E_2 and ν_2, where E and ν are Young's modulus and Poisson's ratio, respectively. In this case the displacement of the inner radius of the casing is

$$u_r^{(1)}(R_1) = \frac{4(1-\nu_1^2)E_2}{N^2(\alpha_2-\alpha_1)+\alpha_1+(1-2\nu_1)\alpha_2} R_1 e_\infty \quad (3)$$

where $N^2 = R_1^2/R_2^2$, $\alpha_1 = E_1(1+\nu_2)$, $\alpha_2 = E_2(1+\nu_1)$, and e_∞ is the far-field radial strain. In general, the strain field is not radially symmetric, so this model was modified for an arbitrary strain field. Figure 8 shows an undeformed and deformed borehole with the spring and contact points of the capsule with respect to the tiltmeter channels. The position of the center of the capsule is defined by noting that the distance between the center and the cavity along the contact points remains equal. That is,

$$|\,\mathbf{c}-\mathbf{r}_2'\,| \;=\; |\,\mathbf{c}-\mathbf{r}_3'\,|\,. \quad (4)$$

The vectors $\mathbf{r}_2'$ and $\mathbf{r}_3'$ are now defined as functions of the strain along the azimuths of the contact points ϵ_2 and ϵ_3. Then the actual strain-induced tilt along the tiltmeter channels is

$$\Omega_x = -\frac{c_r}{30}(\epsilon_2+\epsilon_3) \quad \text{and} \quad \Omega_y = -\frac{c_r}{30\sqrt{3}}(\epsilon_2-\epsilon_3) \quad (5)$$

where

$$c_r \;=\; \frac{4(1-\nu_1^2)E_2}{N^2(\alpha_2-\alpha_1)+\alpha_1+(1-2\nu_1)\alpha_2}. \quad (6)$$

This effect depends upon the installation azimuth and must be included when comparisons between multiple installations of a borehole (along different azimuths) are made. It has been incorporated into the ellipse plots as part of the error ellipses because there is a 180° ambiguity in the orientation of the spring which was not resolved for the early installations.

Table 4 lists the amplitude and phase of the corrections for both tidal frequencies using E_1 = 200 GPa,

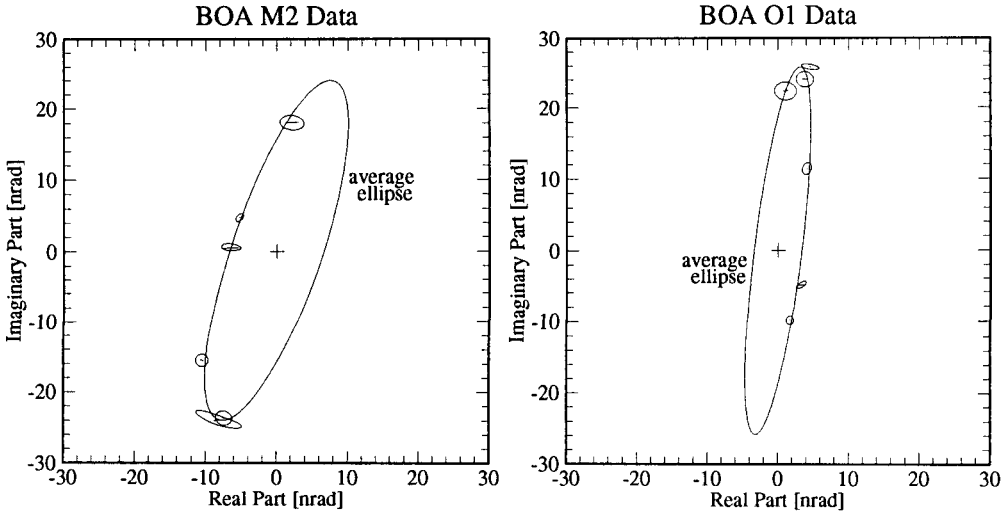

Figure 9. Data from the first three installations of BOA which used the original capsule design. The instrumental effect of the asymmetric springs is included in the error ellipses (small).

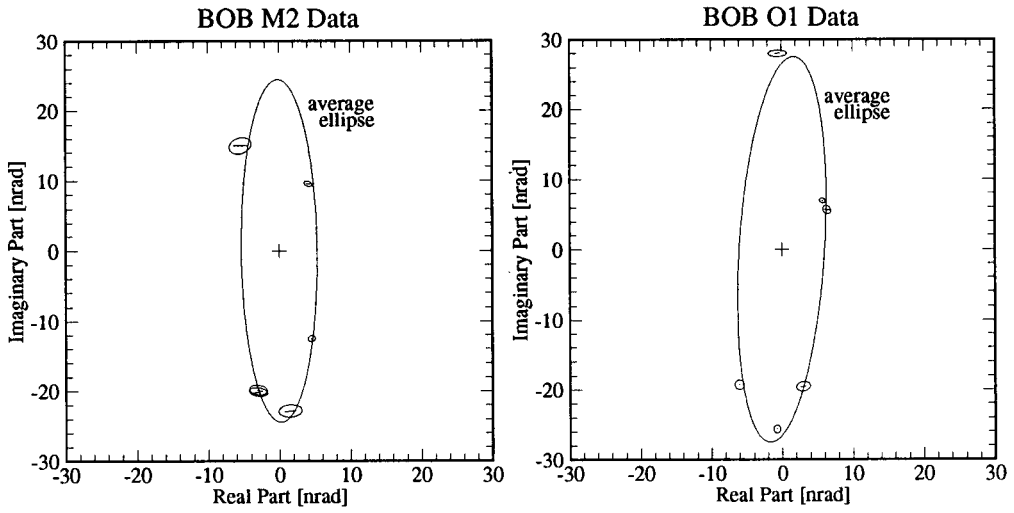

Figure 10. Data from the first three installations of BOB which used the original capsule design. The instrumental effect of the asymmetric springs is included in the error ellipses (small).

$\nu_1 = 0.3$ (values for steel), and $E_2 = 50$ GPa, $\nu_2 = 0.22$ (values for Piñon) [*Wyatt*, 1989]. The magnitude of the instrumental effect orthogonal to the springs (y component) is considerably smaller than the effect along the spring azimuth (x component). The largest absolute magnitude is 1 nrad which is a very small correction to the error ellipses. However, the agreement between the installations of each borehole was improved by accounting for the asymmetric spring on the original capsule. Figure 9 shows the M_2 and O_1 tidal data for these installations of BOA. The ellipse is the average ellipse from the three installations. Figure 10 shows the same plots for the BOB data.

Another instrumental effect is that of an inclined borehole. This effect was calculated by *Agnew* [1986] in three dimensions. Given the angle of inclination as η and the azimuth of inclination as α, the strain-induced tilt from measuring in an inclined borehole Ω^i is

$$\Omega^i_{NS} = \cos\eta \sin\eta(\cos\alpha e_{\theta\theta} + \sin\alpha e_{\theta\lambda} - \cos\alpha e_{rr}) \quad (7)$$

$$\Omega^i_{EW} = \cos\eta \sin\eta(\cos\alpha e_{\theta\lambda} + \sin\alpha e_{\lambda\lambda} - \sin\alpha e_{rr}). \quad (8)$$

Table 5. Strain-Induced Tilt From the Inclined Borehole Model for BOC and the Corrected Average Ellipses

Azimuth, deg	O_1 Amplitude, nrad	O_1 Phase, deg	M_2 Amplitude, nrad	M_2 Phase, deg
		Strain-Induced		
35	0.81	-174.0	2.25	179.6
125	0.11	-104.0	0.33	9.5
		Measured Data		
35	21.61	-81.7	11.92	152.9
125	15.06		23.16	-76.2
		Corrected Data		
35	21.66	-79.5	9.96	147.1
125	14.95	-94.6	23.14	-77.0

The strain-induced tilt along an arbitrary azimuth β is

$$\Omega^i_\beta = \cos\eta \sin\eta \left[\left(\cos\beta\cos\alpha - \frac{1}{2}\sin(\alpha+\beta) - \left(\frac{\nu}{\nu-1}\right)\cos(\alpha-\beta)\right)\epsilon_{NS} + \left(\sin\beta\sin\alpha - \frac{1}{2}\sin(\alpha+\beta) - \left(\frac{\nu}{\nu-1}\right)\cos(\alpha-\beta)\right)\epsilon_{EW} + \sin(\alpha-\beta)\epsilon_{NW}\right] \quad (9)$$

where the strain tensor has been replaced by the strain measured along the azimuths NS, EW, and NW. This strain-induced tilt does not vanish along the azimuth orthogonal to the inclination of the borehole.

BOC is the only borehole for which α and η are known because it was measured using a gyroscope ($\eta \sim 6°$, $\alpha = 210°$). Using the strain tides measured at Piñon Flat (Table 1), the magnitude of the tilt-strain coupling for BOC was calculated. Table 5 lists the strain-induced tilt for the two tidal frequencies M_2 and O_1 (assuming 7° of inclination, $\nu = 0.22$), and the corrected tidal data for BOC. Figure 11 shows the uncorrected and corrected BOC tidal ellipses with respect to the average BOA data. For both frequencies the agreement with the BOA data improves.

While the direction and magnitude of the inclination of the BOA and BOB boreholes are unknown, the sensors can be leveled at the bottom, implying that the inclination of the holes is less than 5°. Corrections to the BOA and BOB ellipses from the inclined borehole cavity effect will be smaller than the calculated correction for BOC. Therefore this effect is too small to fully account for the differences in BOB.

Material Effects

Wyatt [1989] found that a fairly large discontinuity in material properties occurs at Piñon Flat Observatory between 15 and 35 m depth. This type of discontinuity

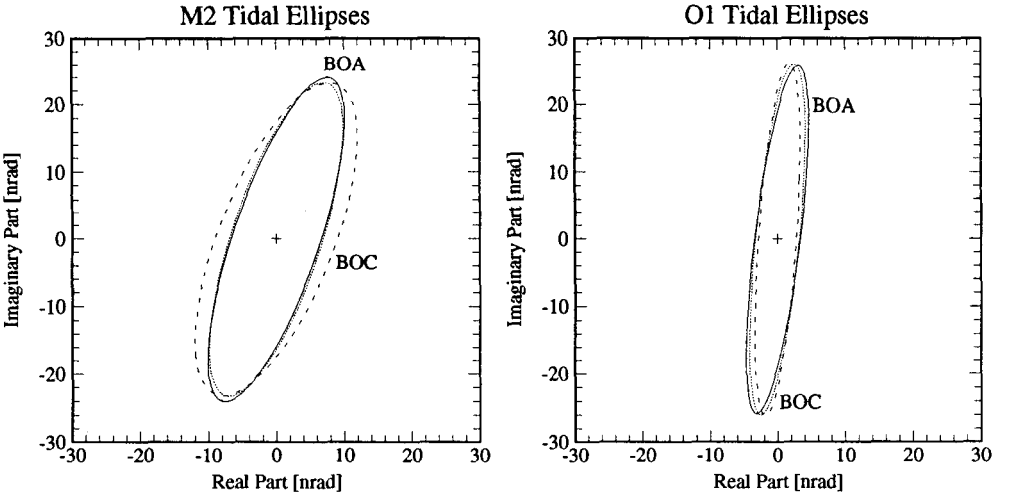

Figure 11. BOC tidal ellipses including the inclined borehole cavity effect compared with BOA. The solid ellipse is the average BOA data using the original capsule. The dashed ellipse is the average BOC data and the dotted ellipse is the BOC data corrected for the inclined borehole cavity effect.

is associated with the weathering of the granite and can be quite abrupt, occurring in the region above the water table [*Stierman and Healy,* 1984]. In order to determine what effect such a discontinuity could have on tidal measurements, we calculated the strain-induced tilt field near a sinusoidal boundary between two regions of different material properties [*Kohl,* 1993]. We found that the strain-induced tilt is discontinuous across the boundary and decreases with increasing distance from the boundary. Figure 12 shows the strain-induced tilt just above and just below a sinusoidal boundary with an amplitude of 0.1 and a wavelength of 2, using the elastic parameters for Piñon Flat [*Wyatt,* 1989]. In this case the strain-induced tilt tides can be as large as 75% of the strain tide.

To determine whether this kind of material effect could be causing the differences seen in the BOB borehole, we modified the tiltmeter capsule, which allowed us to install the instrument at slightly different depths in a borehole. Figure 13 shows the modified capsules located in the borehole. There are two modified capsules; one that rests on the hemisphere at the bottom of the borehole, and one that rests on the joint above the instrument compartment. The first capsule has a plate welded to the bottom of the capsule with a cone cut into it. The cone centers the bottom of the capsule on the hemisphere at the bottom of the hole. The second capsule uses a plate with a spherical edge welded to the bottom that centers on the conical joint in the casing. The top of the modified capsules uses three spring-loaded pins, centering the top of the capsule by equalizing the force on each pin. The new capsules should improve the repeatability of the tidal measurements when rotating the tiltmeter capsule in the borehole, because the instrumental effect described earlier has been significantly reduced [*Kohl,* 1993].

The modified capsules were installed in both the BOA and BOB boreholes. Data from the installations are shown in Tables 6 and 7. The third column indicates which capsule was used for each installation. The data from the BOA borehole at the two different depths are plotted in Figure 14 for the two tidal frequencies M_2 and O_1. It is evident that the data agree between installations within the uncertainties. This result proves that measuring the tilt field using the capsules that locate on the bottom and on the joint does not introduce an instrumental effect. In addition, it shows that there is no perturbation in the tilt field larger that the uncertainty of the measurement near the bottom of the BOA borehole. Therefore a material discontinuity as modeled earlier does not exist near the bottom of the BOA borehole.

The data from the BOB borehole from the two different depths are plotted as tidal ellipses in Figure 15 for the same frequencies. In this case the measured tilt varies significantly at the two depths. This indi-

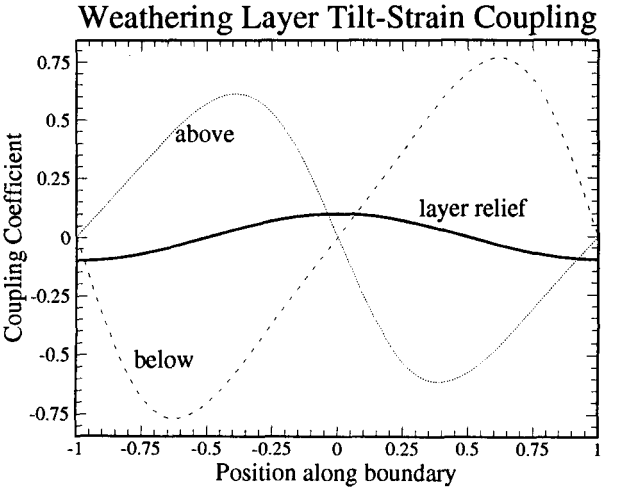

Figure 12. Weathering layer tilt-strain coupling coefficients for a relief defined by $h(x) = 0.1\cos(\pi x)$ and using the elastic parameters from Piñon for the two layers [*Wyatt,* 1989].

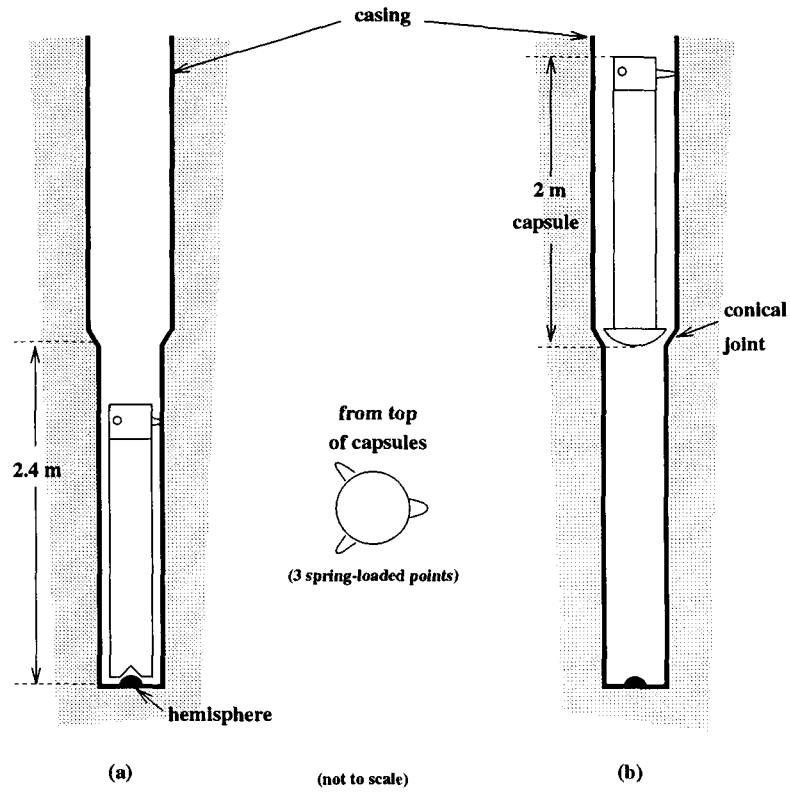

Figure 13. The modified capsules have three spring loaded pins located at the top of the capsule. (a) The first design centers the bottom of the capsule on the hemisphere in the casing while, (b) the second design locates on the conical joint above the instrument compartment.

cates that there is indeed a large perturbation in the tilt field near the bottom of the BOB borehole. Since the data from BOA indicated that there is no instrumental effect introduced by the modified capsules, the most likely cause of the differences is a material effect.

The precise shape and location of the material effect which is causing the perturbation in the tilt field is not known, but the data can be used to help constrain it. Since the analytical model described earlier is a two-dimensional solution, it does not include potentially important cross-coupling features. Therefore a three-dimensional finite element model program was used to investigate the material discontinuity. The accuracy of the finite element model was determined by comparing the results of a radially symmetric strain applied to the model with the results of the two-dimensional analytical solution described above. For this case the finite element program agreed with the analytical results at the 10% level.

A model of a sinusoidal bump separating regions of different material properties was solved. The strain field measured at Piñon Flat by the laser strain meters was applied to the boundaries of the model. The resulting strain-induced tilt throughout the model was then calculated. Provided there is a location on the sinusoidal bump where the strain-induced tilts can account

Table 6. M_2 Data Using the Modified Capsules

			Pendulum 1			Pendulum 2			Uncertainty, %	
Installation	Data Interval, yr:day	Capsule Location	Azimuth, deg	Amplitude, nrad	Phase, deg	Azimuth, deg	Amplitude, nrad	Phase, deg	Ch1	Ch2
				BOA						
4	92:080—92:219	bottom	268	15.09 (0.62)	83.6 (2.4)	358	19.12 (0.94)	113.5 (2.8)	3.5	2.5
5	92:299—93:029	joint	350	21.34 (0.40)	108.2 (1.1)	80	12.67 (0.46)	-98.7 (2.1)	1.0	1.0
				BOB						
4	92:080—92:212	joint	90	14.90 (0.39)	-94.6 (1.5)	0	21.75 (0.23)	122.6 (0.6)	1.0	1.0
5	92:299—93:029	bottom	268	16.31 (0.47)	72.8 (1.7)	358	19.49 (0.24)	93.7 (0.7)	1.6	1.2

Bottom refers to measurements made with the modified capsule at the bottom of the borehole. Joint refers to measurements made ~2.4 m above the bottom of the borehole.

Table 7. O_1 Data Using the Modified Capsules

Installation	Data Interval, yr:day	Capsule Location	Pendulum 1 Azimuth, deg	Pendulum 1 Amplitude, nrad	Pendulum 1 Phase, deg	Pendulum 2 Azimuth, deg	Pendulum 2 Amplitude, nrad	Pendulum 2 Phase, deg	Uncertainty, % Ch1	Uncertainty, % Ch2
				BOA						
4	92:080—92:219	bottom	268	25.23 (0.93)	94.0 (2.1)	358	10.23 (1.29)	-55.8 (7.2)	3.5	2.5
5	92:299—93:029	joint	350	7.01 (0.38)	-51.1 (3.1)	80	26.09 (0.96)	-86.2 (2.1)	1.0	1.0
				BOB						
4	92:080—92:212	joint	90	23.20 (0.35)	-99.1 (0.9)	0	9.83 (0.58)	-67.5 (3.4)	1.0	1.0
5	92:299—93:029	bottom	268	26.55 (0.96)	88.6 (2.1)	358	11.00 (0.67)	-45.2 (3.5)	1.6	1.2

Bottom refers to measurements made with the modified capsule at the bottom of the borehole. Joint refers to measurements made ~2.4 m above the bottom of the borehole.

for the differences measured at the two depths at both the M_2 and O_1 tidal frequencies, the model of a sinusoidal bump is sufficient to describe the material discontinuity. It turns out that such a location along the sinusoidal bump does not exist, which simultaneously accounts for the measured differences at both tidal frequencies. A location can be chosen such that differences measured in the semidiurnal tides are reduced significantly, but then the diurnal frequencies still show significant differences. Likewise, a location which reduces the differences at diurnal frequencies does not improve the semidiurnal results. This implies that the simple model of a sinusoidal bump is insufficient to describe the material discontinuity near BOB.

Discussion

Our results have been compared with results from other instruments at the site. An Askania borehole tiltmeter was installed during the same period in the KUA borehole (see Figure 1) at a depth of 24 m. This tiltmeter is centered in the borehole using three spring-loaded points and the center of the bottom of the borehole [*Agnew*, 1986] which is similar to the modified versions of our capsules. A long fluid tiltmeter (LFT) oriented along 107° azimuth was also operating during this time. Figure 16 shows the BOA tidal ellipses compared to the KUA [*Wyatt and Levine*, 1987] and LFT [*Wyatt et al.*, 1982] results. The data from the Askania tiltmeter agree with the BOA data rather than the BOB data. This is consistent with the existence of a large perturbation in the tilt field near the bottom of the BOB borehole. Also shown are the theoretical ellipses calculated for Piñon Flat Observatory (see Tables 2 and 3) [*Kohl*, 1993]. The theoretical tide includes the ocean load (calculated by Agnew [*Wyatt et al.*, 1982]) and the effects of the topography following the method of *Meertens and Wahr* [1986]. The theoretical tides are significantly different than the BOA measured tides at the M_2 tidal frequency. This could be a result of local geology (not included in the theoretical computation) or errors in the ocean tide models.

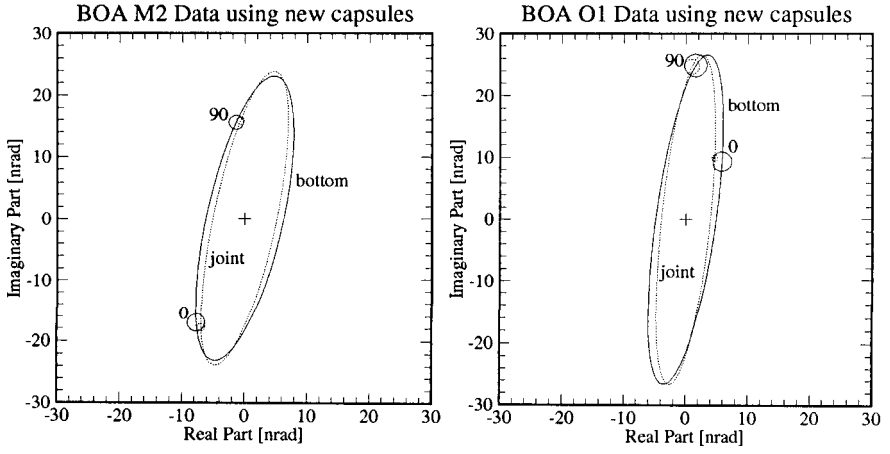

Figure 14. BOA tidal data measured at two different depths using the new capsule designs with the symmetric spring arrangement. The solid ellipse is data obtained from the bottom of the borehole (installation 4), and the dotted ellipse is data obtained from the joint (installation 5). The error ellipses (small) have been rotated to 0° and 90° azimuth for comparison purposes.

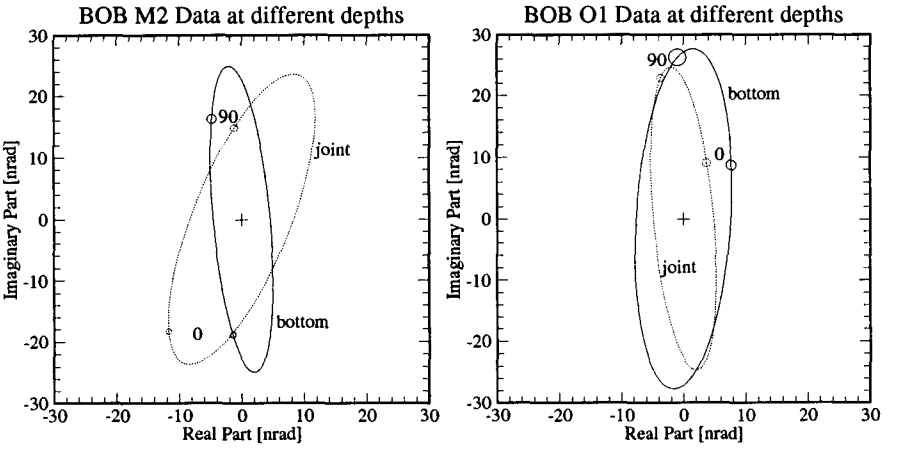

Figure 15. BOB tidal data measured at two different depths using the new capsule designs with the symmetric spring arrangement. The solid ellipse is data obtained from the bottom of the borehole (installation 5), and the dotted ellipse is data obtained from the joint (installation 4). The error ellipses (small) have been rotated to 0° and 90° azimuth for comparison purposes.

Tiltmeters installed at depths of at least 24 m show no evidence of surface effects at Piñon Flat Observatory. The coherence studies indicate that surface effects are minimized when the sensor is installed far from any boundary layers such as a water table. For this reason a drilling log can provide useful information for determining the optimal depth of installation of a tiltmeter in the borehole as well as for interpreting the tilt data.

We have shown that tidal analysis can be used to determine whether a tiltmeter is installed near a material boundary, since variations in material properties can produce large strain-induced tilts near the discontinuity. To do this the tiltmeter must be installed at different depths in a borehole. Measuring the tilt tides at several different depths in a borehole could map out the material discontinuity.

A simple model of a weathering layer at Piñon Flat yields strain-induced tilts large enough to account for the tilt field measured at the bottom of the BOB borehole. However, the model is not sufficient to completely describe the actual material discontinuity which is producing the strain-induced tilt.

It is important to note that the material effects described here are frequency independent and will therefore apply to secular measurements as well. That is, the secular strains will affect the secular tilt measurements with the same coupling coefficients determined for the tides.

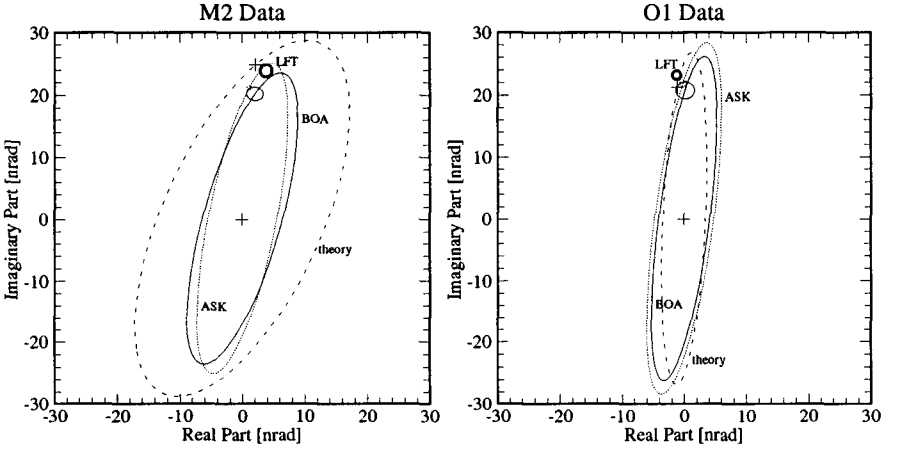

Figure 16. Comparison between the BOA results and other instruments at Piñon Flat. The solid ellipse is the BOA data, the dotted ellipse is data from the Askania tiltmeter in the KUA borehole [*Wyatt and Levine*, 1987], and the dashed ellipse is the theoretical tide (see Tables 2 and 3) [*Kohl*, 1993]. The error ellipses have been rotated to 107° azimuth to compare with the long fluid tiltmeter results shown as the thick error ellipse [*Wyatt et al.*, 1982].

Acknowledgments. We would like to thank Frank Wyatt and Duncan Agnew at IGPP, Scripps Institute of Oceanography, for discussions and help in obtaining the data used here. Leo Weuve was invaluable help in the field. This work was supported in part by the National Earthquake Hazards Reduction Program of the U.S. Geological Survey through grants 14-08-001-G1338 and 14-08-001-G1765.

References

Agnew, D. C., Strain tides at Piñon Flat: Analysis and interpretation, Ph.D.thesis, Univ. of Calif., San Diego, 1979.

Agnew, D. C., Strainmeters and tiltmeters, *Rev. Geophys.*, *24*(3), 579–624, 1986.

Beaumont, C., Tidal loading: Crustal structure of Nova Scotia and the M_2 tide in the northwest Atlantic from tilt and gravity observations, *Geophys. J. R. Astron. Soc.*, *53*, 27–53, 1978.

Beaumont, C., and J. Berger, Earthquake prediction: Modification of the Earth tide tilts and strains by dilatancy, *Geophys. J. R. Astron. Soc.*, *39*, 111–121, 1974.

Cartwright, D. E., and A. C. Edden, Corrected tables of tidal harmonics, *Geophys. J. R. Astron. Soc.*, *33*, 253–264, 1973.

Cartwright, D. E., and R. J. Taylor, New computations of the tide-generating potential, *Geophys. J. R. Astron. Soc.*, *23*, 45–74, 1971.

Evans, K., and F. Wyatt, Water table effects on the measurement of Earth strain, *Tectonophysics*, *108*, 323–337, 1984.

Fletcher,J., T. Fumal, H. Liu and L. Carroll, Near-surface velocities and attenuation at two boreholes near Anza, California, from logging data, *Bull. Seismol. Soc. Am.*, *80*(4), 807–831, 1990.

Harrison, J. C., Cavity and topographic effects in tilt and strain measurement, *J. Geophys. Res.*, *81*(2), 319–328, 1976.

Harrison, J. C., and K. Herbst, Thermoelastic strains and tilts revisited, *Geophys. Res. Lett.*, *4*(11), 535–537, 1977.

Haubrich, R. A., Earth noise, 5 to 500 millicycles per second, *J. Geophys. Res.*, *70*(6), 1415–1427, 1965.

King, G. C. P., and R. G. Bilham, Tilt measurement in Europe, *Nature*, *243*, 74–75, 1973.

Kohl, M. L., Measurement and interpretation of tidal tilts in southern California, Ph.D. thesis, Univ. of Colo., Boulder, 1993.

Kohl, M. L., and J. Levine, Measuring low frequency tilts, *J. Res. Natl. Inst. Stand. Technol.*, *98*(2), 191–202, 1993.

Levine, J., A study of secular tilt in Wyoming and Utah, final report, *Rep. AFGL-TR-83-0247*, Air Force Geophys. Lab., Hanscom AFB, Mass., 1983.

Levine, J., C. Meertens and R. Busby, Tilt observations using borehole tiltmeters, 1, Analysis of tidal and secular tilt, *J. Geophys. Res.*, *94*(B1), 574–586, 1989.

Meertens, C., and J. Wahr, Topographic effect on tilt, strain and displacement measurements, *J. Geophys. Res.*, *91*(B14), 14,057–14,062, 1986.

Meertens, C., J. Levine and R. Busby, Tilt observations using borehole tilmeters, 2, Analysis of data form Yellowstone National Park, *J. Geophys. Res.*, *94*(B1), 587–601, 1989.

Peters, J., and C. Beaumont, Tidal and secular tilt from an earthquake zone: Thresholds for detection of regional anomalies, *Earth Planet. Sci. Lett.*, *84*, 263–276, 1987.

Stierman, D. J., and J. H. Healy, A study of the depth of weathering and its relationship to the mechanical properties of near-surface rocks in the Mojave Desert, *Pure Appl. Geophys.*, *122*, 425–439, 1984.

Wood, M. D., and N. E. King, Relation between earthquakes, weather, and soil tilt, *Science*, *197*, 154–156, 1977.

Wyatt, F., Displacements of Surface Monuments: Horizontal Motion, *J. Geophys. Res.*, *87*(B2), 979–989, 1982.

Wyatt, F., Displacements of surface monuments: Vertical motion, *J. Geophys. Res.*, *94*(2), 1655–1664, 1989.

Wyatt, F., and J. Levine, Side-by-side tidal tilt measurements – some disturbing results (abstract), *Eos Trans. AGU*, *68*, 1247, 1987.

Wyatt, F., G. Cabaniss and D. C. Agnew, A comparison of tiltmeters at tidal frequencies, *Geophys. Res. Lett.*, *9*(7), 743–746, 1982.

Wyatt, F., S. Morrissey and D. C. Agnew, Shallow borehole tilt: A reprise, *J. Geophys. Res.*, *93*(B8), 9197–9201, 1988.

M. L. Kohl, Timing Solutions Corporation, 1025 Rosewood Ave., Suite 200, Boulder, CO 80302. (e-mail: kohlm@strain.colorado.edu).

J. Levine, Joint Institute for Laboratory Astrophysics, University of Colorado, Campus Box 440, Boulder, CO 80309-0440. (e-mail: jlevine@india.colorado.edu).

(Received March 4, 1994; revised October 10, 1994; accepted October 19, 1994.)